

# Critical behavior of a water monolayer under hydrophobic confinement

Valentino Bianco<sup>1</sup> and Giancarlo Franzese<sup>1</sup>

<sup>1</sup>*Departament de Física Fonamental, Universitat de Barcelona, Diagonal 645, 08028 Barcelona, Spain*

(Dated: December 13, 2012)

We study by Monte Carlo simulations the low temperature phase diagram of a water monolayer confined between hydrophobic walls separated by  $h \approx 0.5$  nm. By finite size scaling of the appropriate order parameter, we find a liquid-liquid critical point (LLCP) in the universality class of the two-dimensional (2D) Ising model in the limit of infinite walls. However, for wall sizes up to hundreds of times larger than the monolayer thickness  $h$ , the LLCP is better described by the 3D Ising model universality class, something unexpected based on studies for simple liquids. We ascribe this result to the strong cooperativity and the low coordination number of the hydrogen bond network.

PACS numbers: 64.70.Ja, 65.20.-w, 68.15.+e

The study of nanoconfined water is of great interest for applications in nanotechnology and nanoscience [1]. The confinement of water in quasi-one or two dimensions (2D) is leading to the discovery of new and controversial phenomena in experiments [1–3] and simulations [3, 4]. Nanoconfinement, both in hydrophilic and hydrophobic materials, can keep water in the liquid phase at temperatures as low as 130 K at ambient pressure [2]. At these temperatures  $T$  and pressures  $P$  experiments cannot probe liquid water in the bulk, because water freezes faster than the minimum observation time of usual techniques, resulting in an experimental “no man’s land” [5]. Nevertheless, new kind of experiments [6] and numerical simulations can access this region, revealing interesting phenomena in the metastable state [7]. In particular, Poole et al. found, by molecular dynamics simulations of supercooled water, a liquid-liquid critical point (LLCP), in the “no mans land”, at the end of a first-order liquid-liquid phase transition (LLPT) line between two metastable liquids phases with different density  $\rho$ : the high- $\rho$  liquid at higher  $T$  and  $P$ , and the low- $\rho$  liquid at lower  $T$  and  $P$  [7]. The presence of a LLPT is experimentally observed in other systems [8], consistent with theoretical models fitted to water experimental data [9], and is recovered by simulations of several models of water [7, 10, 11] and other anomalous liquids [12, 13]. Alternative ideas, and their differences, have been discussed [14–16], and experiments on confined water in the “no man’s land” have been seen as a way to test these ideas [2]. Therefore, it is relevant to understand which property, if any, confined water shares with bulk water. Several theoretical works have taken first steps in this direction [17], such as, e.g., analyzing how the increasing of confinement affects the  $T$  and  $\rho$  of the water liquid-gas critical point [18].

Here, to analyze the thermodynamic properties of water in confinement we consider a monolayer of water molecules between hydrophobic walls of area  $L^2$  separated by  $h \approx 0.5$  nm (Fig. 1). Atomistic simulations [4] show that water under these conditions does not crystallize, but arranges in an disordered liquid layer, whose

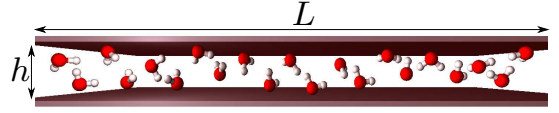


FIG. 1. Schematic view of a section of the water monolayer confined between hydrophobic walls of size  $L \times L$  separated by  $h \approx 0.5$  nm.

projection on one of the surfaces has square symmetry, with each water molecule having four nearest neighbours (n.n.). The molecules maximize their intermolecular distance by occupying different distances from the two walls.

We adopt a model that reproduces water properties [11, 15, 19–22]. The monolayer with  $i = 1, \dots, N$  water molecules, each with four n.n., is partitioned into  $N$  equivalent cells of square section with size  $r \equiv \sqrt{L^2/N}$ , equal to the average distance between water molecules, with  $V \equiv hL^2$ ,  $V/N \geq v_0$ , with  $v_0 \equiv hr_0^2$  ( $r_0 \equiv 2.9\text{\AA}$ ) water excluded volume. By coarse-graining the molecules distance from the surfaces, we reduce our monolayer representation to a 2D system. We use periodic boundary conditions parallel to the walls to reduce finite-size effects. We simulate constant  $N$ ,  $P$ ,  $T$ , allowing  $V(T, P)$  to change, with each cell having density  $\rho_i \equiv \rho(T, P) \equiv N/V \leq \rho_0 \equiv 1/v_0$ . To each cell we associate a variable  $n_i = 0$  ( $n_i = 1$ ) depending if the cell  $i$  has  $\rho_i/\rho_0 \leq 0.5$  ( $\rho_i/\rho_0 > 0.5$ ). The water-water interaction is given by

$$\mathcal{H} \equiv \sum_{ij} U(r_{ij}) - JN_{\text{HB}} - J_{\sigma}N_{\text{coop}}. \quad (1)$$

The first term, summed over all the water molecules  $i$  and  $j$  at O–O distance  $r_{ij}$ , has  $U(r) \equiv \infty$  for  $r < r_0$  (water van der Waals diameter),  $U(r) \equiv 4\epsilon[(r_0/r)^{12} - (r_0/r)^6]$  for  $r \geq r_0$  with  $\epsilon \equiv 1.45$  kJ/mol (van der Waals attraction energy) and  $U(r) \equiv 0$  for  $r > r_c \equiv 25r_0$  (cutoff).

The second term represents the directional (covalent) component of the hydrogen bond (HB), with  $J \equiv 2.9$  kJ/mol,  $N_{\text{HB}} \equiv \sum_{\langle ij \rangle} n_i n_j \delta_{\sigma_{ij}, \sigma_{ji}}$  number of HBs, with the sum over n.n.,  $\sigma_{ij} = 1, \dots, q$  bonding index of  $i$  to  $j$ ,  $\delta_{ab} = 1$  if  $a = b$ , 0 otherwise. Each water molecule

can form up to four HBs. A HB breaks when the OH—O distance  $> r_{\max} - r_{\text{OH}} = 3.14\text{\AA}$ , because  $n_i n_j = 0$  when  $r_{ij} \geq r_{\max} \equiv r_0 \sqrt{2} = 4.10\text{\AA}$  ( $r_{\text{OH}} = 0.96\text{\AA}$ ). Adopting  $q = 6$ , we account correctly for the entropy loss due to HB formation and for the HB breaking if  $\angle \text{OOH} > 30^\circ$ , because only  $1/6$  of the entire range of orientations  $[0, 360^\circ]$  in the OH—O plane is associated to a bonded state.

The third term accounts for the HB cooperativity due to the quantum many-body interaction [23], with  $J_\sigma \equiv 0.29 \text{ kJ/mol}$  and  $N_{\text{coop}} \equiv \sum_i n_i \sum_{(l,k)_i} \delta_{\sigma_{ik}, \sigma_{il}}$ , where  $(l, k)_i$  indicates each of the six different pairs of the four indices  $\sigma_{ij}$  of a molecule  $i$ . To this term is due the O—O—O correlation that locally leads the molecules toward an ordered configuration, that in supercooled bulk water is tetrahedral at low  $P$  up to the second shell [24]. An increase of  $T$  or  $P$  partially disrupts the HB network and induces a more compact local structure, with smaller average volume per molecule. Therefore, for each HB we include an enthalpy increase  $P v_{\text{HB}}$ , where  $v_{\text{HB}}/v_0 = 0.5$  is the average volume increase between high- $\rho$  ices VI and VIII and low- $\rho$  (tetrahedral) ice Ih. Hence, the total volume is  $V \equiv V_0 + N_{\text{HB}} v_{\text{HB}}$ , where  $V_0 \geq N v_0$  is a stochastic continuous variable changing with Monte Carlo (MC) acceptance rule [21]. Because the HBs do not affect the n.n. distance [24], we ignore their negligible effect on the  $U(r)$  term. Finally, we model the water-wall interaction by excluded volume.

We simulate  $\sim 10^5$  state points with statistics of  $5 \times 10^6$  independent calculations for systems with  $N = 2500, \dots, 40000$  water molecules, using a cluster MC algorithm [21], for a wide range of  $T$  and  $P$ , that in real units are as low as  $T = 120 \text{ K}$  and as high as  $P = 0.4 \text{ GPa}$  [19–22]. Here, we adopt as units  $4\epsilon/k_B$  for  $T$  and  $4\epsilon/v_0$  for  $P$ , with  $k_B$  Boltzmann constant.

We find (Fig. 2) (i) a liquid-to-gas spinodal at  $P < 0$  for low  $T$ , (ii) a line of  $T$  of maximum density (TMD) along isobars that approaches the spinodal, without touching it, and continues in the locus (iii) of the line of  $T$  of minimum density (TminD) as in experiments [25] and other models [13, 26]. We calculate the isothermal compressibility  $K_T(T) \equiv -(\partial \ln \langle V \rangle / \partial P)_T$  along isobars, where  $\langle V \rangle$  is the average volume, the isobaric expansivity  $\alpha_P(P) \equiv (\partial \ln \langle V \rangle / \partial T)_P$  and the isobaric specific heat  $C_P(P) \equiv (\partial \langle H \rangle / \partial T)_P$  along isotherms, where  $\langle H \rangle \equiv \langle \mathcal{H} \rangle + P \langle V \rangle$  is the average enthalpy. We verify the thermodynamic equilibrium by checking that the calculation of each quantity by its definition and by the fluctuation-dissipation relation converge. For each quantity we find two maxima at low  $P$ , with higher- $T$  maxima broader and weaker than lower- $T$  maxima [22].

We find that both maxima of  $|\alpha_P|$  along isotherms [locus (iv) of weak maxima  $|\alpha_P|^{\text{wM}}$  and (v) of stronger maxima  $|\alpha_P|^{\text{M}}$ ] coincides within the error bars with the two maxima of  $K_T$  along isobars [locus (vi) of weak maxima  $K_T^{\text{wM}}$  and (vii) of stronger maxima  $K_T^{\text{M}}$ ], consistent with

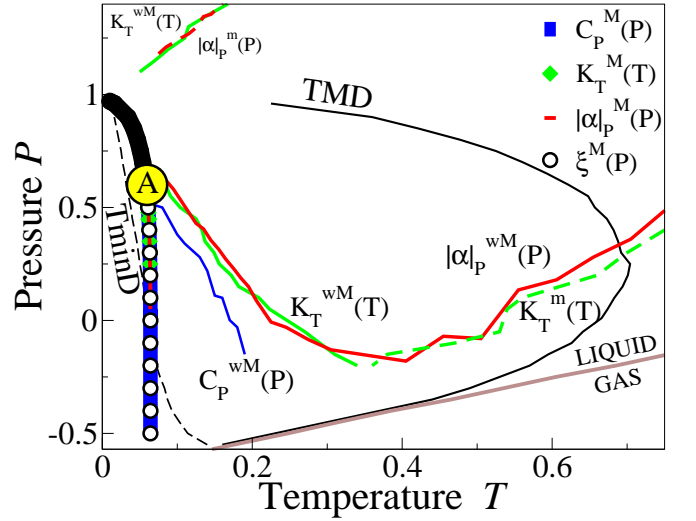


FIG. 2. Phase diagram of  $N = 10^4$  water molecules in a mono-layer nanoconfined between hydrophobic walls. The loci (see text) are marked by lines (full for maxima, dashed for minima) or symbols with labels nearby or in the legend. The liquid-to-gas spinodal (gray line) delimits the region of stability of the liquid with respect to the gas phase. The LLCP (large circle with A) is at the end of the LLPT (thick black) line. Error bars are of the order of the swaying of the lines or the size of the symbols.

thermodynamic relations [14]. This consistency holds also for the locus (iv) intersecting the TMD line in its turning point [14], and for the locus (viii) of weak  $C_P$  maxima ( $C_P^{\text{wM}}$ ) along isotherms bending toward the turning point of the TminD line [26]. The locus (ix) of strong  $C_P$  maxima ( $C_P^{\text{M}}$ ) coincides with loci (v) and (vii). Finally, the loci (iv) and (vi) continue in the loci (x)  $|\alpha_P|^{\text{m}}$  of minima of  $|\alpha_P|$  and (xi)  $K_T^{\text{m}}$  of minima of  $K_T$  where  $dP/dT$  along these loci is infinite or zero [13, 26], respectively (not shown in Fig.2).

All the loci of maxima of response functions (iv)-(ix) converge toward the point A. Moreover, all the maxima along these loci increase in their values by approaching the point A. Because the increase of response functions is related to the increase of fluctuations and this is, in turn, related to the increase of correlation length  $\xi$ , we calculate the spatial correlation function  $G(r_{il}) \equiv \langle \sigma_{ij}(\vec{r}_i) \sigma_{lk}(\vec{r}_l) \rangle - \langle \sigma_{ij} \rangle^2$  to estimate  $\xi$ . We find that for  $P$  below the point A,  $G(r)$  decays as an exponential with a characteristic correlation length  $\xi$ . For  $P$  approaching the point A,  $G(r)$  is better approximated by a power-law decay with an exponential prefactor from which  $\xi$  can be extracted. At the point A, the exponential prefactor approaches a constant leaving the power-law as the dominant contribution for the decay, corresponding to  $\xi$  becoming of the order of the system size. We observe that  $\xi$  has a maximum along isobars and that the Widom line, i.e. the locus (xii) of maxima  $\xi^{\text{M}}$ , coincides with the loci (v), (vii) and (ix). All these observations

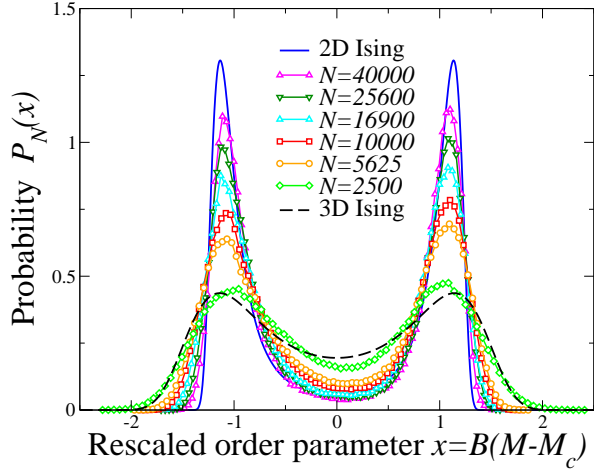


FIG. 3. The size-dependent probability distribution  $P_N$  for the rescaled order parameter  $x$ , calculated for  $T_c(N)$ ,  $P_c(N)$  and  $B(N)$  in Fig. 4, has a symmetric shape that approaches continuously (from  $N = 2500$ , symbols at the top at  $x = 0$ , to  $N = 40000$ , symbols at the bottom) the limiting form for the 2D Ising universality class (full line), maximizing the difference with the 3D Ising universality class (dashed line). Lines connecting the symbols are guides for the eye. Error bars are smaller than the symbols size.

[convergence of loci (iv)-(ix) and (xii) and the increase of maxima along these loci on approaching  $A$ ] are consistent with the identification of  $A$  with a LLC at the end of a first-order LLPT line in the  $P$ - $T$  phase diagram along which the density, the energy and the entropy of the liquid are discontinuous, as discussed in previous works [11, 15, 19–22]. Next, we analyze in detail the LLC.

According to mixed-field finite-size scaling theory [27], a density-driven fluid–fluid phase transition is described by an order parameter  $M \equiv \rho + su$ , where  $\rho$  represents the leading term,  $u$  is the energy density (both in internal units) and  $s$  is the field mixing parameter. At the critical point the probability distribution of  $M$  is  $P_N(M) \propto \tilde{p}_d(x)$ , i.e. scales as an universal function  $\tilde{p}_d$ , characteristic of the Ising fixed point in  $d$  dimensions, of  $x \equiv B(M - M_c)$ , where  $B \equiv a_M^{-1} N^{\beta/d\nu}$ ,  $\beta$  is the  $M$  critical exponent,  $\nu$  is the  $\xi$  critical exponent, both defined by the universality class, and  $a_M$  is a non-universal system-dependent parameter. We adjust  $B$  and  $M_c$  so that  $P_N(M)$  has zero mean and unit variance.

By combining a set of  $3 \times 10^4$  MC simulations for  $\sim 300$  state points with  $0.033 \leq T \leq 0.065$  and  $0.01 \leq P \leq 0.90$  with the multiple histogram reweighting method [28], and tuning  $s$ ,  $T$  and  $P$  we verify that in the vicinity of the state point  $A$  the calculated  $P_N(x)$  has a symmetric shape with respect to  $x = 0$  (Fig. 3). We find  $s = 0.25 \pm 0.03$  for our range of  $N$ . The resulting critical parameters  $T_c(N)$ ,  $P_c(N)$  and the normalization factor  $B(N)$  follow in fair agreement the expected finite-size behaviors with 2D Ising critical exponents [27] (Fig. 4).

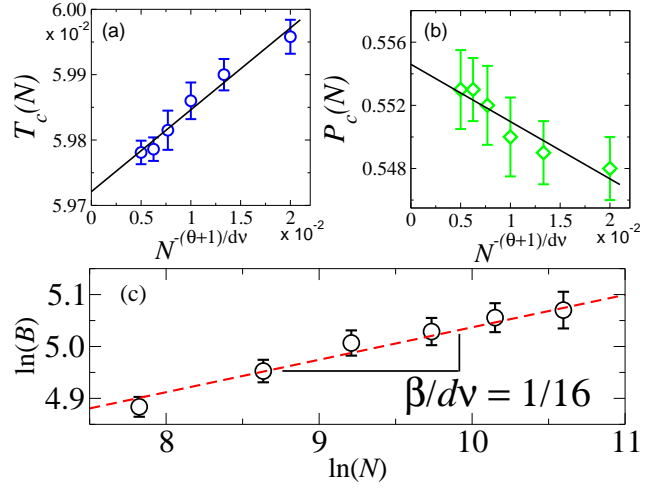


FIG. 4. The size-dependent LLC temperature  $T_c(N)$  (a) and pressure  $P_c(N)$  (b) (symbols), used for best-fitting  $P_N$ , extrapolate to  $T_c \simeq 0.0597$  and  $P_c \simeq 0.554$ , respectively, following the expected linear behaviors (lines). (c) The normalization factor  $B(N)$  (symbols) follows the power law function (dashed line)  $\propto N^{\beta/d\nu}$ . We use the  $d = 2$  Ising critical exponents:  $\theta = 0$ ,  $\nu = 1$  and  $\beta = 1/8$ .

From the finite-size analysis we extract the asymptotic values  $T_c = 0.0597 \pm 0.0001$  and  $P_c = 0.554 \pm 0.003$ , consistent with the state point  $A$ . However, these fits adjust well to the data only for large  $N$ . We, therefore, perform a more systematic analysis.

For each  $N$ , we quantify the deviation of the calculated  $\tilde{p}(N)$  from the expected  $\tilde{p}_2$  for the 2D Ising. Furthermore, due to the behavior of data for small  $N$  in Fig. 3, we calculate the deviation from the 3D Ising  $\tilde{p}_3$  [27]. Following Liu et al. [18], we define the deviation from each  $\tilde{p}_d$  as

$$W_d(N) \equiv \frac{1}{n} \frac{\sum_{i=1}^n \sqrt{\tilde{p}_i(N)} |\tilde{p}_i(N) - \tilde{p}_{d,i}|}{\tilde{p}_{d,\text{peak}} - \tilde{p}_{d,x=0}}, \quad (2)$$

with  $n$  total number of points for  $x$ ,  $\tilde{p}_i(N)$  probability distribution of  $x_i$ ,  $\tilde{p}_{d,i}$  theoretical value for  $x_i$ ,  $\tilde{p}_{d,\text{peak}} - \tilde{p}_{d,x=0}$  difference between the distribution peak and its value at  $x = 0$ .

We confirm  $s \simeq 0.25$  for  $\tilde{p}_2$  and find  $s = 0.10 \pm 0.02$  for  $\tilde{p}_3$  for our range of  $N$ . For both  $W_2$  and  $W_3$  we find minima that become stronger for increasing  $N$  and are always close to  $T_c \simeq 0.06$  and  $P_c \simeq 0.55$ , i.e. at approximately constant  $\rho_c$ . We find that  $W_2$  decreases with increasing  $N$ , being as low as 0.046 for  $N = 4 \times 10^4$ , with  $W_2(N) \rightarrow 0$  for  $N \rightarrow \infty$  (Fig. 5). Therefore, for an infinite monolayer confined between hydrophobic walls separated by  $h \approx 0.5$  nm, the system has a LLC that belongs to the 2D Ising universality class, consistent with our coarse-graining of the monolayer in 2D.

However, by increasing the confinement, i.e. reducing  $N$  and  $L$  at constant  $\rho$ ,  $W_2$  becomes larger than  $W_3$ . The difference  $W_2 - W_3$  increases with decreasing  $N$ , and for

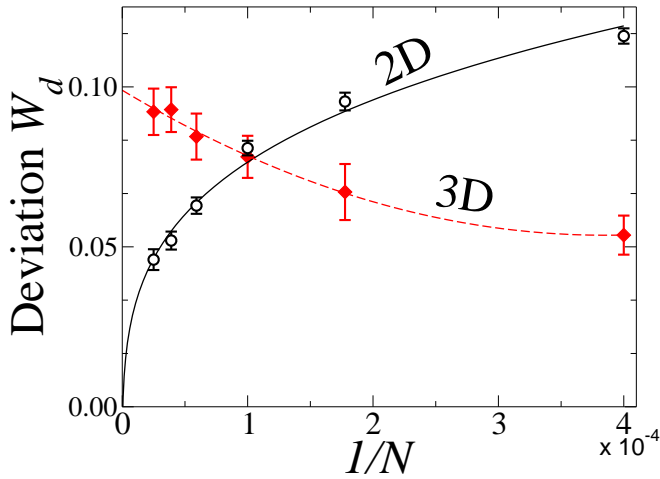


FIG. 5. Deviations  $W_d$  of the calculated  $\tilde{p}(N)$  from the  $d = 2$  (open symbols) and  $d = 3$  (closed symbols) Ising universal function  $\tilde{p}_d$ , as function of the inverse of the number of water molecules  $N$  at constant  $\rho \simeq \rho_c$ . Lines are power-law fits.

$N = 2500$  is  $W_3 \simeq W_2/3 \simeq 0.05$ , a value approximately equal to the smallest  $W_2$  we find for a system ten times larger. In other words, by increasing the confinement of the monolayer at constant  $\rho$ , the LLCPC has a behavior that approximates better the bulk [10], with a crossover between 2D and 3D-behavior occurring at  $N \simeq 10^4$ .

This dimensional crossover is confirmed by the finite-size analysis of the Gibbs free energy cost  $\Delta G/(k_B T_c)$  to form an interface between the two liquids in the vicinity of the LLCPC, calculated as  $\Delta G(N) \equiv -k_B T_c(N)[\ln P_N(x=0) - \ln P_N(x_{\text{MAX}})]$ , with  $P_N$  reaching a maximum at  $x_{\text{MAX}}$ . This quantity is expected to scale as  $\Delta G \propto N^{\frac{d-1}{d}}$ . We find that our data can be fitted as  $N^{\frac{2}{3}}$  for small sizes and as  $N^{\frac{1}{2}}$  for large sizes with a crossover around  $N = 10^4$  (Fig. 6). Considering the value of the estimated  $\rho_c$  in real units ( $\simeq 1\text{g/cm}^3$ ) [20], the corresponding crossover wall-size is  $L \simeq 75\text{ nm}$ .

Our rationale for this dimensional crossover at fixed  $h$  is that, when  $h/L$  increases, the characteristic way the critical fluctuations spread over the system, i.e. the universality class of the LLCPC, resembles closely the bulk because the asymmetry among the three spatial dimensions is reduced. A similar result was found recently by Liu et al. for the gas-liquid critical point of a Lennard-Jones (LJ) liquid confined between walls by fixing  $L$  and varying  $h$  [18]. However, in the case considered by Liu et al. the crossover was expected because the number of layers of particles was increased from one to several, making the system more similar to the isotropic 3D case. Here, instead, we consider always one single layer, changing the proportion  $h/L$  by varying  $L$  instead of  $h$ . Therefore, it could be expected that the system belongs intrinsically to the 2D universality class for any  $L$ .

Furthermore, the extrapolation of the results for the LJ liquid to the case of a monolayer with  $h/r_0 \simeq 1.7$ ,

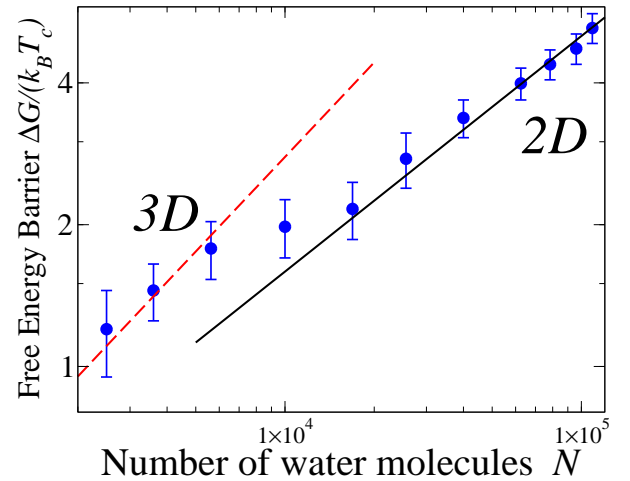


FIG. 6. The free-energy cost to form an interface between the two liquids coexisting at the LLCPC scales as  $\Delta G \propto N^{\frac{d-1}{d}}$  with  $d = 3$  for  $N < 10^4$  and  $d = 2$  for  $N > 10^4$ .

as in our case, would predict a dimensional crossover at  $L/h \lesssim 5$  [18]. For our water monolayer, instead, we find the crossover at  $L/h \simeq 150$ , i.e. two orders of magnitude larger than the LJ case. This implies that the presence of a cooperative HB network and its low coordination number, the main differences between water and a LJ fluid, enhance drastically the spreading of the critical fluctuations along a network that at least for the first shell is similar to the one in 3D, lifting the effective dimensionality of the confined monolayer.

In conclusion, we analyze the low- $T$  phase diagram of a water monolayer confined between hydrophobic parallel walls of size  $L$  separated by  $h \approx 0.5\text{ nm}$ . We identify many loci of the phase diagram, the Widom line, the LLPT and the LLCPC. We show that the LLCPC belongs to the 2D Ising universality class only for  $L/h \geq 150$ . For smaller  $L$  at the same  $\rho$ , i.e. for stronger confinement, the LLCPC is better described by 3D, bulk-like, critical behavior, as a consequence of the high cooperativity and low coordination number of the HB network.

We acknowledge the support of Spanish MEC grant FIS2009-10210 co-financed FEDER and the EU FP7 grant NMP4-SL-2011-266737.

- 
- [1] M. Majumder et al., Nature **438**, 44 (2005); D.R. Paul, Science **335**, 413 (2012); L. Guillemot et al., Proc. Natl. Acad. Sci. USA **109**, 19557 (2012).
  - [2] Y. Zhang et al., Proc. Natl. Acad. Sci. USA **108**, 12206 (2011); **108**, E1193 (2011); A. Soper, *ibid.* E1192 (2011).
  - [3] M. Whitby, and N. Quirke, Nat Nano **2**, 87 (2007).
  - [4] R. Zangi and A.E. Mark, Phys. Rev. Lett. **91**, 025502 (2003); P. Kumar et al., Phys. Rev. E **72** 051503 (2005). M. Sharma et al., Nano Lett. **8**, 2959 (2008); R.R. Nair et



- al. Science **335**, 442 (2012).
- [5] O. Mishima and H. E. Stanley, Nature **396**, 329 (1998).
  - [6] A. Nilsson private communication.
  - [7] P. Poole et al., Nature **360**, 324 (1992).
  - [8] Y. Katayama et al., Nature **403** 170 (2000); Science **306**, 848 (2004); G. Monaco et al., Phys. Rev. Lett. **90** 255701 (2003); H. Tanaka et al., Phys. Rev. Lett. **92**, 025701 (2004); R. Kurita and H. Tanaka, Science **306**, 845 (2004); G. N. Greaves et al., Science **322**, 566 (2008); K.-i. Murata and H. Tanaka, Nature Mater. **11**, 436 (2012); H. Tanaka, Eur. Phys. J. E **35** 113 (2012).
  - [9] C. E. Bertrand and M. A. Anisimov, J. Phys. Chem. B **115**, 14099 (2011); V. Holten et al., J. Chem. Phys. **136** 094507 (2012); V. Holten and M. A. Anisimov, Sci. Rep. **2**, 713 (2012).
  - [10] H. Tanaka, Nature **380**, 328 (1996); J. L. F. Abascal and C. Vega, J. Chem. Phys. **133**, 234502 (2010); F. Sciortino et al., Phys. Chem. Chem. Phys., **13**, 19759 (2011); T. Kesselring et al., Sci. Rep. **2**, 474 (2012); Y. Liu et al., J. Chem. Phys. **137**, 214505 (2012); P. H. Poole et al. arXiv:1212.1600 (2012).
  - [11] G. Franzese et al., Phys. Rev. E **67**, 011103 (2003).
  - [12] Franzese et al., Nature **409**, 692 (2001); S. Sastry and C. A. Angell, Nature Mater. **2**, 739 (2003); S. Scandolo Proc. Natl. Acad. Sci. USA **100** 3051 (2003); P. Ganesh and M. Widom, Phys. Rev. Lett. **102**, 075701 (2009); A. B. de Oliveira et al., J. Chem. Phys. **124**, 084505 (2006); *ibid.* **128**, 064901 (2008); C. W. Hsu et al. Proc. Natl. Acad. Sci. USA **105** 13711 (2008); P. Vilaseca and G. Franzese, J. Non-Cryst. Sol. **357**, 419 (2011); P. Gallo and F. Sciortino, Phys. Rev. Lett. **109**, 177801 (2012).
  - [13] V. V. Vasisht et al. Nature Phys. **7**, 549 (2011);
  - [14] S. Sastry et al., Phys. Rev. E **53**, 6144 (1996).
  - [15] K. Stokely et al., Proc. Natl. Acad. Sci. USA **107**, 1301 (2010).
  - [16] D. T. Limmer and D. Chandler, J. Chem. Phys. **135**, 134503 (2011).
  - [17] A. L. Ferguson et al. J. Chem. Phys. **137**, 144501 (2012). For a recent collection of review papers see, e.g., P. Gallo and M. Rovere *Special section on water at interfaces* J. Phys.: Cond. Matt. **22** 280301 (2010).
  - [18] Y. Liu et al., J. Chem. Phys. **132**, 144107 (2010).
  - [19] P. Kumar et al., Phys. Rev. Lett. **100**, 105701 (2008).
  - [20] F. de los Santos and G. Franzese, J. Phys. Chem. B **115**, 14311 (2011); Phys. Rev. E **85**, 010602(R) (2012).
  - [21] M.G. Mazza et al., Comp. Phys. Comm. **180**, 497 (2009); E.G. Strekalova et al., Phys. Rev. Lett. **106**, 145701 (2011); G. Franzese et al., Food Biophys. **6**, 186 (2011); V. Bianco et al., J. Biol. Phys. **38**, 27 (2012).
  - [22] M.G. Mazza et al., Proc. Natl. Acad. Sci. USA **108**, 19873 (2011); J. Chem. Phys. **137**, 204502 (2012).
  - [23] R. Ludwig, Angew. Chem. Int. Ed. **40**, 1808 (2001); L. Hernández de la Peña and P.G. Kusalik, J. Am. Chem. Soc. **127**, 5246 (2005).
  - [24] A. K. Soper and M. A. Ricci, Phys. Rev. Lett. **84**, 2881 (2000).
  - [25] F. Mallamace et al., Proc. Natl. Acad. Sci. USA **104**, 18387 (2007).
  - [26] P. H. Poole et al., J. Phys.: Cond Matt **17**, L431 (2005).
  - [27] A.D. Bruce and N.B. Wilding, Phys. Rev. Lett. **68** 193 (1992); N.B. Wilding, Phys. Rev. E **52**, 602 (1995); R. Hilfer and N.B. Wilding, J. Phys. A **28**, L281 (1995); N. B. Wilding and K. Binder, Physica A **231**, 439 (1996).
  - [28] A.Z. Panagiotopoulos, J. Phys.: Cond. Matt. **12**, R25 (2000) for a review.